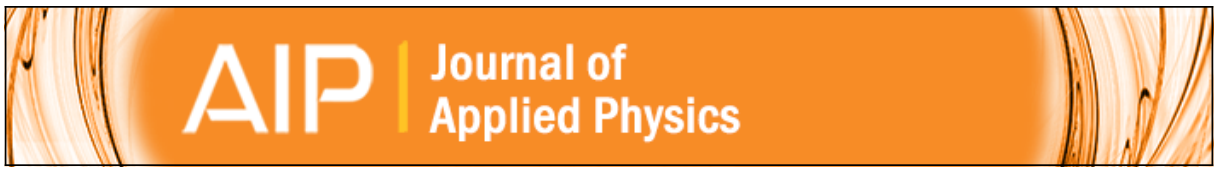


# Lattice thermal conduction in ultra-thin nanocomposites

Iorwerth O. Thomas and G. P. Srivastava

Citation: Journal of Applied Physics **119**, 244309 (2016); doi: 10.1063/1.4954678

View online: http://dx.doi.org/10.1063/1.4954678

View Table of Contents: http://scitation.aip.org/content/aip/journal/jap/119/24?ver=pdfcov

Published by the AIP Publishing



# Lattice thermal conduction in ultra-thin nanocomposites

Iorwerth O. Thomas[a] and G. P. Srivastava
*School of Physics, University of Exeter, Stocker Road, Exeter EX4 4QL, United Kingdom*

(Received 14 February 2016; accepted 11 June 2016; published online 27 June 2016)

We have studied the lattice thermal conductivity of Si/Ge periodic nanocomposites (superlattice, nanowire, and nanodot structures) of sample sizes in the range of 30 nm–30 $\mu$m, periodicities 1.1 nm and 2.2 nm, with reasonably dirty interfaces, and n-type doping concentration in the range of $10^{23}$–$10^{26}$ m$^{-3}$. Our calculations employ a judicious combination of *ab initio* and physically sound semi-empirical methods for detailed calculations of estimates of phonon scattering rates due to anharmonicity and interface formation. Based upon our results we conclude that the formation of ultra-thin nanocomposites in any of the three structures is capable of reducing the conductivity below the alloy limit. This can be explained as a result of combination of the sample length dependence, the on-set of *mini-Umklapp* three-phonon processes, mass mixing at the interfaces between Si and Ge regions, and the sample doping level. *Published by AIP Publishing.*
[http://dx.doi.org/10.1063/1.4954678]

## I. INTRODUCTION

Investigation of lattice thermal conduction in nanostructures and nanocomposites is important, both scientifically and technologically. On one hand, nanostructuring of a material is capable of producing thermal conductivity larger than that of the corresponding bulk material. Clear examples are carbon nanotubes[1] and graphene,[2] whose thermal conductivities are larger than that of bulk diamond. On the other hand, nanostructures and nanocomposites have been reported to produce thermal conductivity values that can be lower than that of alloys or amorphous materials (see, e.g., Ref. 3). Clearly, from technological point of view, the lattice thermal conductivity of such structures is capable of playing an important role at several levels. In this work we will consider a composite structure as a periodic insertion of one material in a homogeneous matrix of another material. We will further use the terminologies "nanocomposite" and/or "nanocomposite superlattices" for such periodic structures with sample sizes in the large nanometer to low micron range and periodicity in the low nanometer range.

One important area of technological applications of reduced thermal conductivity is thermoelectricity. Thermoelectric (TE) materials have potential applications in power generation and refrigeration, resulting from their ability to interconvert thermal gradients and electric fields. The TE properties of a material are usually discussed in terms of its figure of merit $ZT$, which describes its TE efficiency and is defined as

$$ZT = \frac{\sigma S^2 T}{\kappa_{tot}}, \tag{1}$$

where $\sigma$ is the electrical conductivity, $S$ is the Seebeck coefficient (or thermopower), and $\kappa_{tot}$ is the total thermal conductivity. The total thermal conductivity $\kappa_{tot}$ can be expressed as $\kappa_{tot} = \kappa_{el} + \kappa_{ph}$, where the electronic part $\kappa_{el}$ is the sum of the charge carrier (electron or hole) and bipolar (electron and hole) contributions, and $\kappa_{ph}$ is the lattice (phonon) thermal conductivity. Theoretical studies[4–6] have indicated that there should be no real upper limit to $ZT$. However, over the past several decades it has been found that heavily doped semiconductor alloys are the best TE materials, with $ZT \leq 1$.[7,8] Doped BiTeSe, PbTeSe, and SiGe provide examples of low-, intermediate-, and high-temperature TE systems, respectively. However, some commercial applications of TE devices require greater efficiency in order to be viable. It has been apparent since the 1990s that this goal could be reached through the use of low-dimensional nanocomposite materials,[7,9–16] where nano-scale structures of different materials are interwoven in a variety of different ways. It has long been maintained that phonon properties in such structures are likely to play a key role in enhancing $ZT$.[4,8,13,17] In particular, Slack[17] has suggested that materials prepared using techniques which produce glass-like hugely reduced lattice thermal conductivity $\kappa_{ph}$ without significantly reducing the power factor $PF = S^2\sigma$, should help enhance $ZT$. Experimental studies[10,18] have clearly indicated the role of strong interface scattering of phonons in generating large reduction in $\kappa_{ph}$ for thin-period superlattice (SL) structures. However, no full-scale and accurate calculations of phonon scattering rates and conductivity for nanocomposites of different dimensionalities and different volume fractions have been carried out that assess the full extent of the role of phonons in the enhancement of $ZT$ with a high degree of confidence.

Increasing $ZT$ is more difficult than it might seem: while it seems that this could be done by increasing $S$ and $\sigma$ and decreasing $\kappa_{el}$, in practice these quantities are not independent, so that increasing $\sigma$ increases $\kappa_{el}$ and increasing $S$ will typically reduce $\sigma$. Whether or not $ZT$ increases depends then on the complex relationship between these quantities. Despite the effort involved in its calculation, $\kappa_{ph}$ plays a more simple and direct role in determining $ZT$. It should also be noted that $\kappa_{ph}$ is typically large for bulk Si than for bulk

[a]Current Address: Department of Physics, University of Durham, South Road, Durham DH1 3LE, United Kingdom.

Ge.[19] There are therefore two main lines of attack when attempting to improve *ZT* via nanostructuring: one concentrating on improving the power factor $\sigma S^2$ beyond the enhancement arising from a reduction in dimensionality, and another focusing on reducing the phonon thermal conductivity. Venkatasubramanian *et al.*[10] demonstrated the effectiveness of dimensionality-driven reduction in the phonon (lattice thermal) conductivity for $Bi_2Te_3/Sb_2Te_3$ superlattices. Broido and Reinecke[20] found that the increased carrier scattering rates that occur with increasing confinement in superlattice structures cause the power factor $S^2\sigma$ to remain near the bulk value for all barrier heights. Attempts to further improve the power factor through techniques such as carrier pocket engineering are viable but more difficult to implement experimentally.[15,21]

In this work we concentrate on the role of phonons in enhancing *ZT*, as a decrease in $\kappa_{ph}$ is somewhat easier to engineer in real systems. Si/Ge flat plate superlattices of periodicities 4 nm and thicker have been successfully fabricated by many groups using the molecular beam epitaxy method.[22–25] It is hoped that nanowire (NW) and nanodot (ND) composite structures similar to those studied in this work can be fabricated using techniques such as matrix encapsulation[26] and spinodal decomposition and nucleation.[27] The thermal conductivity of Si/Ge nanocomposite superlattices of periodicities 4 nm and thicker has also been measured.[22–25] Theoretical efforts have been made to examine the role of nanocomposite superlattice structure formation with periodicities much thicker than 5 nm in achieving thermal conductivity below the alloy limit.[28–30,32–36] More recently, a systematic study of the size and dimensionality dependent phonon conductivity of PbTe-PbSe nanocomposites (flat plate superlattices, embedded nanowires, and embedded nanodots) of thicker periodicities (100 nm and larger) has been made in the framework of an effective medium theory.[37] Such simplified theoretical schemes are very highly dependent on the use of empirically adjusted phonon interaction parameters in order to fit the thermal conductivities of the bulk materials comprising the nanocomposites and cannot be routinely applied to predict results for ultrathin-period nanocomposite structures of different symmetries, different periodicities, and varying interface qualities. More fundamentally, use of bulk-derived phonon relaxation rates makes these theoretical approaches inapplicable for structures with repeat period sizes smaller than the phonon mean free path (typically smaller than 10 nm).[38] Using reasonable arguments but assuming constant mean free paths ($\Lambda$) of the phonons, Simkin and Mahan[39] have shown that the conductivity of (flat plate) superlattices has a minimum value for a layer thickness somewhat smaller than $\Lambda$. In addition to the lack of full-scale Brillouin-zone integration that considers the full phonon spectrum and an accurate treatment of phonon anharmonic interactions involving all phonon branches in the presence of two (or more) materials in every unit cell, such theoretical approaches do not incorporate the important effects of atomic-level impurities and defects at the internal boundaries (interfaces) in such structures. To the best of our knowledge there has been no publication of a study incorporating an *ab initio* or semi-*ab initio* theoretical formalism of phonon anharmonic interactions in order to calculate the lattice thermal conductivity of nanocomposites of different symmetries and sizes using a single computational approach. This primarily is due to a lack of thorough investigation of two mechanisms of phonon scattering: that due to interface formation and that due to anharmonicity in the presence of more than one material. In the present work our calculations of $\kappa_{ph}$ address these two types of phonon-interface scattering mechanism by using the semi-empirical extension of *ab initio* techniques that we have outlined previously in Refs. 40–44. This is intermediate between the traditional approaches that treat crystals as an isotropic continuum (see, e.g., Ref. 45) and more recent attempts[46,47] to calculate the $\kappa_{ph}$ using wholly *ab initio* approaches that are not yet fully mature. We have justified our choice of approach in Refs. 42 and 44; our approach is capable of picking out which nanostructures provide sufficient improvements to $\kappa_{ph}$ to be worthy of a more intensive investigation that examines both their phononic and electronic properties in exhaustive detail in order to obtain an accurate calculation of *ZT*.

In this paper we detail our formalism for the phonon-interface and three-phonon interaction rates and evaluate the lattice thermal conductivity for Si/Ge nanocomposites of sample sizes in the range 30 nm–30 $\mu$m, ultrathin periodicities 1.1 nm and 2.2 nm, and n-type doping concentration in the range $10^{23}$–$10^{25}$ m$^{-3}$. In particular, we consider three types of nanocomposite structures: (flat plate) Si/Ge[001] superlattices, rectangular Si nano-wires embedded in a Ge host, and cubic Si nanodots embedded in a Ge host. $\kappa_{ph}$ was examined for undoped ultrathin-period superlattices of various thicknesses in our earlier study;[44] here we focus on the effects of doping and sample size on the thermal conductivity of a superlattice with a thickness that (in the undoped case) gives an optimum (i.e., low) $\kappa_{ph}$ in the cross-barrier direction, and compare these effects with those seen in embedded dots and wires of similar sizes. This allows us to examine the influence of the structure of the system (e.g., the presence of interfaces) on $\kappa_{ph}$, and draw some conclusions as to how best to enhance *ZT* by reducing $\kappa_{ph}$ through nanostructuring.

## II. METHOD

The lattice thermal conductivity tensor $\kappa_{ph}$ (also expressed in this work as $\kappa$ for simplicity) within the single-mode relaxation time approximation is given by[48]

$$\kappa_{\mu\nu} = \frac{\hbar^2}{N_0 \Omega k_B T^2} \sum_{\boldsymbol{q}s} \omega^2(\boldsymbol{q}s) c_{s,\mu}(\boldsymbol{q}) c_{s,\nu}(\boldsymbol{q}) \tau(\boldsymbol{q}s) \bar{n}_{\boldsymbol{q}s}(\bar{n}_{\boldsymbol{q}s} + 1), \tag{2}$$

where $N_0$ is the number of unit cells, $\Omega$ is the volume of a unit cell, $\omega(\boldsymbol{q}s)$ and $c_{s,\mu}(\boldsymbol{q})$ are, respectively, the frequency and the velocity component in the $\mu$th direction of the phonon mode with wave vector $\boldsymbol{q}$ and polarization $s$, $\bar{n}_{\boldsymbol{q}s}$ is the equilibrium Bose–Einstein distribution for that mode, and $\tau(\boldsymbol{q}s)$ is the relaxation time of phonon in mode $\{\boldsymbol{q}s\}$. For a nanostructure the total phonon relaxation time is obtained by

summing scattering rates from boundary (bs), point defects (including isotopic mass defects) (md), donor electrons in n-doped samples (ep), interface mass mixing (ims), and anharmonicity (anh): $\tau(\boldsymbol{qs})^{-1} = \tau_{\rm bs}^{-1} + \tau_{\rm md}^{-1} + \tau_{\rm ep}^{-1} + \tau_{\rm ims}^{-1} + \tau_{\rm anh}^{-1}$. The scattering rates $\tau_{\rm bs}^{-1}$, $\tau_{\rm md}^{-1}$, and $\tau_{\rm ep}^{-1}$ were computed using the well-established expressions for bulk semiconductors.[42,48] We also took the carrier concentration to be approximately $N_d$, since scattering from impurity donor electrons should be dominant in the low temperature regions where $\tau_{\rm ep}^{-1}$ is important, and we included frequencies of up to $170\,{\rm cm}^{-1}$ in our calculation of $\tau_{\rm ep}^{-1}$, which should include most of the important contributions from the acoustic modes. $\tau_{\rm ims}^{-1}$ was calculated using the current version[43] of our approach to interface mass-mixing effects,[40,41,43] and is discussed in what follows, as is the calculation of the anharmonic contribution $\tau_{\rm anh}^{-1}$, for which we use a generalization of the approach given in Ref. 43; we also correct some errors in previous statements of these equations.

The present study is restricted to ultra-thin Si/Ge nanocomposite structures in the form of superlattice (SL), embedded nanowire (NW), and embedded nanodot (ND). The considered unit cells and atomic positions are shown in Figure 1 for the SL structure, Figure 2(a) for the NW structure, and Figure 2(b) for the ND structure. The embedding in NW and ND is of Si (atoms of higher thermal conductivity material) in Ge matrix (atoms of lower thermal conductivity material).

### A. Anharmonic scattering

In order to properly describe the anharmonic contribution to the phonon relaxation time in a periodic nanocomposite material, we follow[48,49] and explicitly derive expressions for the Fourier components of the third-order interatomic force constant tensor. The essence of this approach is easily grasped through examining the eigenvalue equation of diatomic linear chain connected with a real-space force constant $\Lambda$, considered as a one-dimensional superlattice with a unit cell of size $2\,a$ containing two atomic species of masses $m_1$ and $m_2$. The eigenvalue equation for such a system can be written as $\omega^2 \boldsymbol{A} = \Phi \boldsymbol{A}$, where $\Phi$ is a $2 \times 2$ dynamical matrix and $\boldsymbol{A}$ is a two-component column matrix describing the detachment amplitudes of the two atoms in the unit cell. An element of the dynamical matrix $\Phi_{ij}$ can be expressed as[48]

$$\begin{aligned}\Phi_{ij} &= \frac{2\Lambda}{m_i} - \frac{2\Lambda}{m_j}\left(\frac{m_j}{m_i}\frac{A_j}{A_i}\cos qa\right), \\ &= \frac{2\Lambda_{\rm eff}}{m_i},\end{aligned} \tag{3}$$

with $A_i$ and $A_j$ as the displacement amplitudes of the atoms of masses $m_i$ and $m_j$, respectively. The first term of the effective force constant $\Lambda_{\rm eff}$ in the above equation, $2\Lambda/m_i$, is simply the dynamical matrix for the monoatomic linear chain with atomic mass $m_i$, i.e., for the $i$-th species of the superlattice. The second term shows that the dynamical matrix for the $j$-th species $(2\Lambda/m_j)$ is phase-multiplied by $\frac{m_j}{m_i}\frac{A_j}{A_i}\cos qa$. Similar phase-related expression(s) for effective force constants will exist in superlattices of realistic dimensions. Thus, the Fourier components of the third-order force constant tensor must also exhibit suitable phase relationships between the atomic vibrational amplitudes of the various material segments of a composite material.

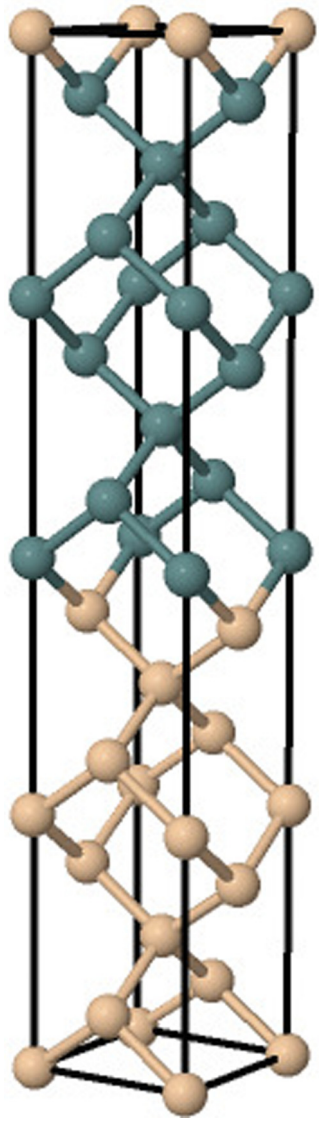

FIG. 1. Atomic structure representation of the Si(4)Ge(4)[001] SL. Gold and blue-gray spheres represent Si and Ge atoms, respectively. Figures were generated using Jmol.[57]

Although in the rest of this article we will adopt a form of cubic anharmonic continuum potential that accounts for both acoustic and optical phonons, for the purpose of explaining our extension of the cubic part of the Hamiltonium in order to account for a two-component composite, we will follow Ref. 48 and write the cubic anharmonic potential for a single-component isotropic elastic continuum as

$$\begin{aligned}V_3 = \frac{1}{3!}\sum_{\boldsymbol{qs},\boldsymbol{q}'s',\boldsymbol{q}''s''} &\left(a^{\dagger}_{\boldsymbol{qs}} - a_{-\boldsymbol{qs}}\right)\left(a^{\dagger}_{\boldsymbol{q}'s'} - a_{-\boldsymbol{q}'s'}\right) \\ &\times \left(a^{\dagger}_{\boldsymbol{q}''s''} - a_{-\boldsymbol{q}''s''}\right)\mathcal{F}(\boldsymbol{qs},\boldsymbol{q}'s',\boldsymbol{q}''s'')\delta_{\boldsymbol{G},\boldsymbol{q}+\boldsymbol{q}'+\boldsymbol{q}''},\end{aligned} \tag{4}$$

with $\mathcal{F}(\boldsymbol{qs},\boldsymbol{q}'s',\boldsymbol{q}''s'')$ expressed as

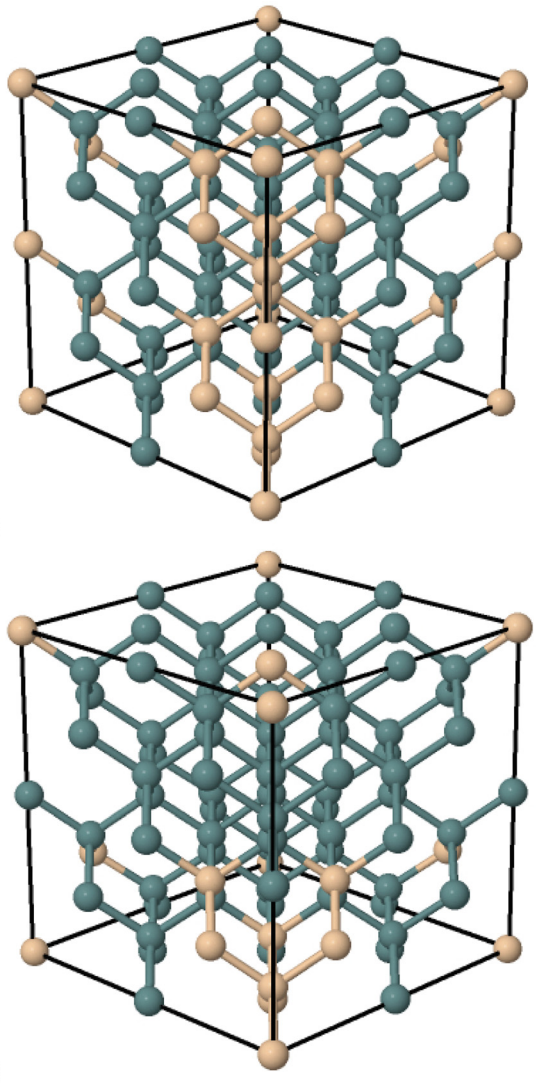


FIG. 2. Atomic structure representation of (a) Si nanowire embedded in Ge host and (b) Si nanodot embedded in Ge host. Gold and blue-gray spheres represent Si and Ge atoms, respectively. Figures were generated using Jmol.[57]

$$\mathcal{F}(\boldsymbol{q}s,\boldsymbol{q}'s',\boldsymbol{q}''s'') = \sqrt{\frac{1}{8\rho^3 N_o \Omega}}\frac{\sqrt{\omega\omega'\omega''}}{cc'c''}A(\boldsymbol{q}s,\boldsymbol{q}'s',\boldsymbol{q}''s''), \tag{5}$$

where $A(\boldsymbol{q}s,\boldsymbol{q}'s',\boldsymbol{q}''s'')$ is a Fourier component of the third-order elastic constants tensor $\{A^{lmn}_{ijk}\}$

$$A(\boldsymbol{q}s,\boldsymbol{q}'s',\boldsymbol{q}''s'') = \sum_{lmn} A^{lmn}_{ijk} e_l e'_m e''_n \hat{\boldsymbol{q}}_i \hat{\boldsymbol{q}}'_j \hat{\boldsymbol{q}}''_k, \tag{6}$$

where $\boldsymbol{e} \equiv \boldsymbol{e}(\boldsymbol{q}s) \equiv \boldsymbol{e}(\boldsymbol{r}|\boldsymbol{q}s)$, etc., are the displacement vectors at point $\boldsymbol{r}$ in the medium. These contain some periodic function of $\mathbf{q}$ and a lattice spacing that is analogous to the $\cos qa$ term in the case of the diatomic lattice discussed above.

Following the discussion above for the diatomic linear chain, we seek to express $A(\boldsymbol{q}s,\boldsymbol{q}'s',\boldsymbol{q}''s'')/\rho^{3/2}$ for a two-component continuum in terms of a set of $n_1$ patches of density $\rho_1$ and $n_2$ patches of density $\rho_2$ in the form:

$$\frac{A(\boldsymbol{q}s,\boldsymbol{q}'s',\boldsymbol{q}''s'')}{\rho^{3/2}} \to \frac{A(\boldsymbol{q}s,\boldsymbol{q}'s',\boldsymbol{q}''s'')}{(n_1+n_2)^3} \times \left(\frac{e_1 e'_1 e''_1}{\rho_1^{3/2}}\mathcal{A}_{12} + \frac{e_2 e'_2 e''_2}{\rho_2^{3/2}}\mathcal{A}_{21}\right), \tag{7}$$

where the quantities $A_{ij}$ are defined as

$$\mathcal{A}_{ij} = \frac{\Gamma_i \rho_i^{3/2}}{e_i e'_i e''_i}\left(\frac{n_1 e_1}{\rho_1^{1/2}} + \frac{n_2 e_2}{\rho_2^{1/2}}\right)\left(\frac{n_1 e'_1}{\rho_1^{1/2}} + \frac{n_2 e'_2}{\rho_2^{1/2}}\right) \times \left(\frac{n_1 e''_1}{\rho_1^{1/2}} + \frac{n_2 e''_2}{\rho_2^{1/2}}\right), \tag{8}$$

with $\Gamma_1$ and $\Gamma_2 = 1 - \Gamma_1$ being the relative proportions of species 1 and 2, respectively. Replacing both $e_1 e'_1 e''_1$ and $e_2 e'_2 e''_2$ with an overall average $e_{\mathrm{AVG}} e'_{\mathrm{AVG}} e''_{\mathrm{AVG}}$ we may then, by comparing the approximate relation[48]

$$\overline{|A(\boldsymbol{q}s,\boldsymbol{q}'s',\boldsymbol{q}''s'')|^2} = \frac{4\rho_0^2}{\bar{c}^2}\gamma^2 cc'c'' \tag{9}$$

with Eq. (7), define a dual mass term $\mathcal{D}(\boldsymbol{q},\boldsymbol{q}',\boldsymbol{q}'')$, given by

$$\mathcal{D}(\boldsymbol{q},\boldsymbol{q}',\boldsymbol{q}'') = \frac{1}{(n_1+n_2)^6}\left(\frac{\mathcal{A}_{12}}{\rho_1^{3/2}} + \frac{\mathcal{A}_{21}}{\rho_2^{3/2}}\right)^2. \tag{10}$$

The values of $n_1$ and $n_2$ for the systems we are (or have been) interested in can be determined by the following procedure. We divide each system into $D$-dimensional sections of equal size (i.e., containing an equivalent number of atoms) and identical species, and take $n_1$ to be the number of sections containing atoms of species 1 and $n_2$ to be the number of sections containing atoms of species 2. This can be illustrated most easily with reference to the $(n, n)$ superlattices which can be divided into two sections, both consisting of $n$ atoms of species 1 and species 2, and hence $n_1 = 1$ and $n_2 = 1$. This results in the form of $\mathcal{D}(\boldsymbol{q},\boldsymbol{q}',\boldsymbol{q}'')$ used in previous studies (Refs. 42 and 43; see also the earlier, less adequate discussion of this term given in Ref. 50). With a little thought, it can be seen from Figure 2 that for the nanowire system that we consider in this paper, $n_1 = 1$ and $n_2 = 3$, whereas for the nanodot we have $n_1 = 1$ and $n_2 = 7$.

For a two-component composite A/B made from materials A and B, we use the following expression for the anharmonic scattering rate, taken and corrected from our previous work:[43]

$$\tau^{-1}_{\mathrm{anh}}(\boldsymbol{q}s) = \frac{\pi\hbar\gamma^2\rho_0^2}{N_0\Omega\bar{c}^2}\sum_{\boldsymbol{q}'s',\boldsymbol{q}''s'',\boldsymbol{G}}\frac{\left(\mathcal{R}_{\boldsymbol{q}s,\boldsymbol{q}'s',\boldsymbol{q}''s''}\right)^2}{\omega(\boldsymbol{q}s)\omega(\boldsymbol{q}'s')\omega(\boldsymbol{q}''s'')}\mathcal{D}(\boldsymbol{q},\boldsymbol{q}',\boldsymbol{q}'') \times \left[\frac{\bar{n}_{\boldsymbol{q}'s'}(\bar{n}_{\boldsymbol{q}''s''}+1)}{(\bar{n}_{\boldsymbol{q}s}+1)}\delta\big(\omega(\boldsymbol{q}s)+\omega(\boldsymbol{q}'s')-\omega(\boldsymbol{q}''s'')\big) \times \delta_{\boldsymbol{q}+\boldsymbol{q}',\boldsymbol{q}''+\boldsymbol{G}} + \frac{1}{2}\frac{\bar{n}_{\boldsymbol{q}'s'}\bar{n}_{\boldsymbol{q}''s''}}{\bar{n}_{\boldsymbol{q}s}} \times \delta\big(\omega(\boldsymbol{q}s)-\omega(\boldsymbol{q}'s')-\omega(\boldsymbol{q}''s'')\big)\delta_{\boldsymbol{q}+\boldsymbol{G},\boldsymbol{q}'+\boldsymbol{q}''}\right]. \tag{11}$$

Here for the composite material $\rho_0$ is the density, $\gamma$ is mode-averaged Grüneisen's constant, $\bar{c}$ is the average of the speeds of the acoustic branches, and

$$\mathcal{R}_{i,j,k} = [\sqrt{\omega(i)\omega(j)}(\omega(i)+\omega(j))|\omega_\Gamma(k)-\omega(k)| + \text{similar terms with } i, j \text{ and } k \text{ interchanged}]/3!, \quad (12)$$

where $\omega_\Gamma(k)$ is the frequency for phonon branch $k$ at the Brillouin zone centre (the $\Gamma$ point), $i, j, k$ label various $\{\boldsymbol{q}\,s\}$, while the effects of nanostructuring are accounted for by the dual-mass term $\mathcal{D}(\boldsymbol{q}, \boldsymbol{q}', \boldsymbol{q}'')$, which, as discussed above, depends on the ratio $\frac{e_B}{e_A}$ of the amplitudes of the vibration in the two materials inside a unit cell of the system. The sums over the zero reciprocal vector $\boldsymbol{G}=0$ and the finite reciprocal vectors $\boldsymbol{G}\neq 0$ account for momentum conserving (Normal) and momentum non-conserving (Umklapp) three-phonon processes, respectively. Periodic composite structures are characterized with $\boldsymbol{G}$ vectors that can be mapped with the reciprocal lattice vectors of the constituent bulk materials as well as some new, and smaller than bulk, reciprocal lattice vectors. The presence of the latter set can be described to produce "mini-Umklapp" processes.[49] For the amplitude ratio, we use an approximation based on a generalization of the linear chain model (see, for example, Refs. 48 and 51)

$$\frac{e_B}{e_A} = \frac{\left[\frac{1}{M_0} - \Delta\left(\frac{1}{M}\right)\right]\sum_\mu \cos(q_\mu l_\mu)}{\left[\left(\frac{d}{M_0}\right)^2 + \frac{\mathcal{A}}{M_A M_B}\right]^{1/2} - d\Delta\left(\frac{1}{M}\right)},$$
$$\mathcal{A} = d^2 - \left(\sum_\mu \cos(q_\mu l_\mu)\right)^2, \quad (13)$$

where $M_0 = (M_A^{-1}+M_B^{-1})/2$ and $\Delta(1/M) = (M_A^{-1} - M_B^{-1})/2$; $M_{A(B)}$ is the mass of species A(B) and $l_\mu$ is *half* the length of the cell in the direction $\mu$, and $d$ represents the number of phonon confinement directions due to composite structuring. The phase relationship encoded in the dual-mass term must reflect the periodicity of the nanostructure in question. This means that in Eq. (13), for superlattices we set $d=1$ and sum only over $\mu=z$, for nanowires we set $d=2$ and sum only over $\mu=x, y$ and for quantum dots we set $d=3$ and sum over $\mu=x, y, z$.

### B. Interface mass-smudging (IMS) scattering

For an ultra-short-period nanocomposite A/B, we treat interface scattering to solely arise from mass mixing (i.e., mass swapping) across the interface between the materials A and B in each unit cell. With A/B taken as Si/Ge, we consider mass swapping between diamond-structure bi-layers across an interface within each nanocomposite unit cell. We use the approach of Ref. 43 in order to treat phonon scattering due to interface mass mixing (IMS scattering) in superlattice structures. It is generalized to the case of three-dimensional (3D) cells in the Appendix to this paper. Accordingly, the IMS scattering rate for a phonon $\boldsymbol{q}s$ can be written as

$$\tau_{ims}^{-1}(\boldsymbol{q}s) = \frac{\pi\Gamma_{\text{ims}}}{6N_0}\sum_{\boldsymbol{q}'s'}\omega(\boldsymbol{q}s)\omega(\boldsymbol{q}'s')\delta\big(\omega(\boldsymbol{q}s)-\omega(\boldsymbol{q}'s')\big) \times \frac{(\bar{n}_{\boldsymbol{q}'s'}+1)}{(\bar{n}_{\boldsymbol{q}s}+1)}, \quad (14)$$

with

$$\Gamma_{\text{ims}} = \mathcal{P}^2\left(\frac{\Delta M}{M}\right)^2\left(\left[1-\frac{e_A e_A'}{e_B e_B'}\right]^2 + \left[1-\frac{e_B e_B'}{e_A e_A'}\right]^2\right), \quad (15)$$

where $\mathcal{P}$ is the overall probability of a pair of atoms (i.e., atoms in a bi-layer in species A exchanging with some pair of atoms (i.e., atoms in a bi-layer) in species B and is dependent on some choice of two parameters: $\mathcal{B}$ and $\alpha$. Essentially, $\alpha$ controls the probability of a bilayer exchange across an interface and $\mathcal{B}^\alpha$ controls the probability of interchange for adjacent bilayers. For this scattering rate we should use a definition of the amplitude ratio $e_B/e_A$ that is consistent with the nature of the cell we are discussing: only one-dimensional exchange is meaningful for the simple superlattice (SL) cell that we examine, so we take $\mu=z$; for both the nanodot and nanowire cells used here the bilayer exchange can occur in all three directions, so we take $\mu=x, y, z$.

### C. Calculation of phonon eigensolutions

The phonon dispersion relations and phonon velocity components in the Si/Ge nanocomposite structures were computed by employing the *ab-initio* density-functional perturbation theory as implemented in the Quantum Espresso package.[52] We utilized the local density approximation and norm-conserving pseudopotentials,[53] and a plane wave basis up to the kinetic energy cutoff of 15 Ry. Brillouin zone summations required for calculations of electronic structure, phonon frequencies, phonon velocities, and phonon scattering rates were performed using the Monkhorst–Pack (MP) special wave-vectors method.[54] The chosen energy cutoff is sufficient to obtain reasonably well converged results for phonon frequencies and velocities.[55] It is well established that the mode-average Grüneisen constant $\gamma$ generally increases with temperature $T$. For $T>150\,\text{K}$, we made the choice $\gamma_0\left(1+\frac{(T-150)}{150}\right)^{0.56}$, taking the SL value[43] $\gamma_0=0.45$ for all of the nanostructures; this value is also consistent with the experimental data for SiGe alloys.[56]

The unit cell for the Si/Ge[001] superlattice was constructed with the basis vectors $\boldsymbol{a}_1 = a_{\text{SL}}(1/\sqrt{2}, 0, 0)$, $\boldsymbol{a}_2 = a_{\text{SL}}(0, 1/\sqrt{2}, 0)$, and $\boldsymbol{a}_3 = a_{\text{SL}}(0, 0, 4)$, with a lattice constant $a_{\text{SL}}$. Each unit cell, shown in Fig. 1, contains 8 Si atoms (4 bilayers) and 8 Ge atoms (4 bilayers). The cubic lattice constant was chosen to be $a_{\text{SL}}=5.54\,\text{Å}$, the average of the experimental lattice constants of bulk Si and bulk Ge, in accordance with Vegard's law. With this lattice constant, relaxed inter-atomic bond lengths were calculated employing the force minimization technique. For this system, the energy minimization and dynamical matrix calculation were performed on a $10\times10\times2$ MP grid and the phonon eigensolutions were derived from those using a $16\times16\times12$ MP grid, which gives reasonably good numerical convergence.[43] All allowed three-phonon Normal processes, as well as Umklapp processes involving reciprocal lattice vectors up to magnitude $G = 2\times 2\pi/a_{\text{SL}}$, were included.

The periodic embedded NW and ND structures were constructed by using the basis vectors $\boldsymbol{a}_1 = a_{\mathrm{NW,ND}}(2,0,0)$, $\boldsymbol{a}_2 = a_{\mathrm{NW,ND}}(0,2,0)$, and $\boldsymbol{a}_3 = a_{\mathrm{NW,ND}}(0,0,2)$, with the lattice constants $a_{\mathrm{NW,ND}}$. The nanowire unit cell contains 16 Si atoms and 48 Ge atoms (Fig. 2(a)), and the nanodot unit cell contains 8 Si atoms and 56 Ge atoms (Fig. 2(b)). The relaxed inter-atomic bond lengths were determined. The cubic lattice constants of $a_{\mathrm{NW}} = 5.56$ Å and $a_{\mathrm{ND}} = 5.59$ Å for the nanowire and the nanodot structures, respectively, were determined using Vegard's law. Numerically converged thermal conductivity results for these systems are computationally prohibitive for us, due to the large number of $\boldsymbol{q}$-points needed to do so and due to the parallelization constraints of the Quantum Espresso package.[58] This renders a search for a $\boldsymbol{q}$-point converged $\tau_{\mathrm{anh}}$ as unfeasible at this point since such a converged system would require many $\boldsymbol{q}$-points. Instead a Monkhorst–Pack grid of $4 \times 4 \times 4$ was used for both systems. For this reason our results should be taken to be exploratory rather than final. Phonon quantities were calculated using eigensolutions generated on the 20 $\boldsymbol{q}$-point grid and symmetry rotations of the nanowire in order that we might compare systems that are as similar as possible. The shortest 18 reciprocal lattice vectors were used for the nanodot and 32 for the nanowire; beyond this value the Umklapp scattering saturates.

## III. RESULTS

We first present a brief analysis and discussion of the $\kappa_{\mathrm{ph}}$ results for the [001] superlattice structure. We note that Si/Ge SL structures are characterized by large structural mismatch (compared with Si, bulk Ge is characterized by a lattice mismatch of ≈4%, a mass ratio of 2.58, and a density ratio of 2.29) and that the resulting phonon spectrum for the ultra-thin SLs is very different from those of bulk Si and Ge.[40] In particular, branches become flatter and several phononic gaps appear in the spectrum, giving rise to changes in the anharmonic relaxation rate of phonon modes. Although ultra-thin Si/Ge superlattices do not appear to contain many dislocations,[22,59,60] mass-smudging occurs in a rather unpredictable and uncontrolled manner, dependent upon growth conditions and preparation methods,[24] and will have a noticeable effect on the lattice thermal conductivity: "dirtier" interfaces with more mass-mixing will give rise to a greater reduction in $\kappa_{\mathrm{ph}}$ than "cleaner" interfaces since in the former case the phonon-interface scattering is stronger. Note that a "dirty" enough interface is likely to cause the system to behave like a phonon glass where electrons are still affected by the underlying crystal structure. Figure 3 shows the computed results for the components of the lattice thermal conductivity tensor for a "dirty" interface (modeled with the interface mass-smudging scattering parameters $\alpha = 2$ and $\mathcal{B} = 1$ using the notation described in the Appendix and in Ref. 43) for the (4,4) SL (periodicity 2.2 nm along [001]) with sample length $L = 3.0 \times 10^{-7}$ m and n-type P-doping of various concentrations.

The results at room temperature and above for both the in-plane components $\kappa_{\mathrm{ph}}^{xx}$ and $\kappa_{\mathrm{ph}}^{yy}$ are significantly lower than the typical values for bulk Si or bulk Ge (see, e.g., Ref. 19).

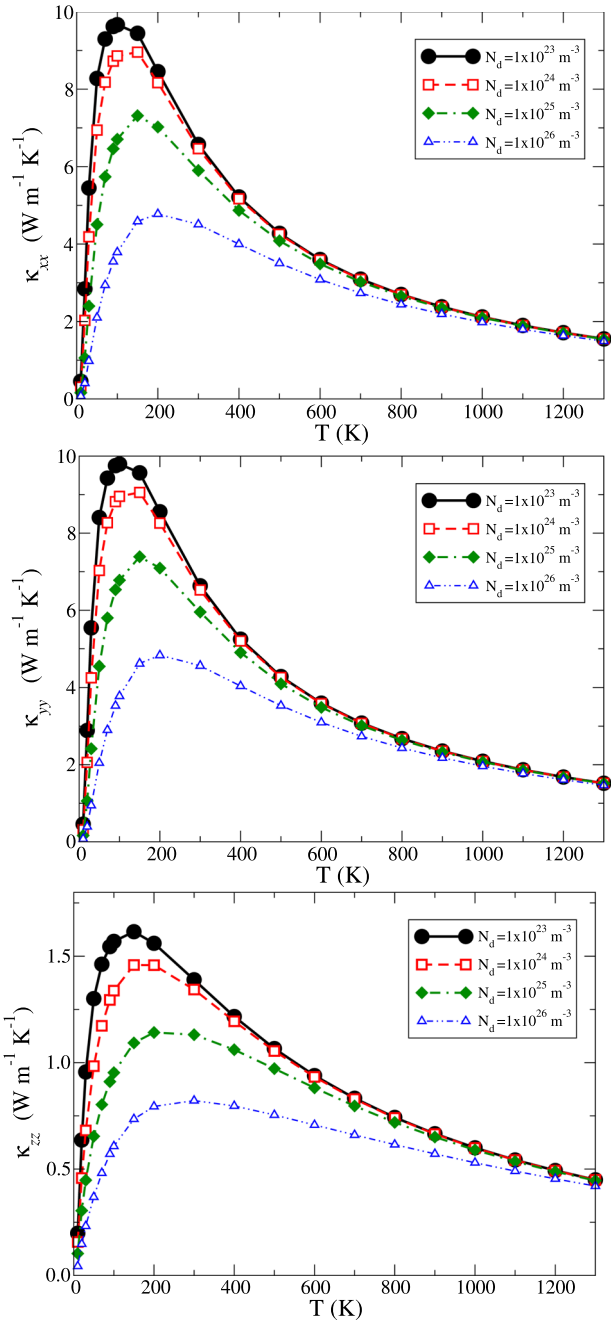


FIG. 3. Components of the lattice thermal conductivity tensor $\kappa_{\mathrm{ph}}$ for the Si(4)Ge(4)[001] superlattice when $L_B = 3 \times 10^{-7}$ m, $\alpha = 2.0$, and $\mathcal{B} = 1.0$ (see text and Ref. 43 for notation).

The cross-planar component $\kappa_{\mathrm{ph}}^{zz}$ shows an even more significant reduction, typically more than two orders of magnitude lower than the values for bulk Si or bulk Ge, and also significantly lower than results obtained previously by us for the $Si_{0.75}Ge_{0.25}$ alloy[42] even for dopant concentrations that are orders of magnitude smaller than that of the sample considered in that study, where $\kappa_{\mathrm{ph}}$ was the dominant contribution to the thermal conductivity. This is consistent with the intuition that thermal conduction in the growth direction (and so across interfaces) will be more affected by the presence of interfaces than thermal conduction in the planar directions where the thermal current will not cross interfaces. Qualitatively, $\kappa_{\mathrm{ph}}^{xx}$ and $\kappa_{\mathrm{ph}}^{yy}$ are similar but not quite identical;

this small discrepancy arises from our choice of the [110] and [1$\bar{1}$0] directions as $x$ and $y$ and is discussed in Ref. 44. In general, the effect of increasing carrier concentration $N_d$ is to decrease $\kappa_{ph}$ at low temperatures; as we reach high temperatures the values for different concentrations tend to converge, as scattering processes other than electron-phonon scattering become dominant, although for $\kappa_{ph}^{zz}$ the $N_d = 10^{26}\,m^{-3}$ results remain noticeably smaller than the rest. Our prediction of the conductivity of these ultrathin-period Si/Ge (flat plate) superlattices in the sub-1 W m$^{-1}$ K$^{-1}$ region is consistent with previously reported results in this range from other groups for thicker-period superlattices.[30] However, a direct numerical comparison of the results for different periodicity sizes, and obtained by employing different levels of theory, would be inappropriate. Recently, Garg and Chen[31] computed the thermal conductivity of Si/Ge superlattices using an *ab initio* theoretical formalism similar to that of ours. The results presented in this paper as well as in our previous work[43] for the 2.2 nm period Si/Ge superlattice are similar to the results obtained by Garg and Chen.[31] However, a detailed numerical comparison of our results with the Garg–Chen results cannot be made. This is because Garg and Chen considered an undoped sample, did not specify the sample length, and did not clearly specify the interface mass-mixing region.

Figure 4 displays the effects of doping on the lattice contribution to the thermal conductivity for both the nanowire and the nanodot structures. In general, we see a decrease of the thermal conductivity as both the doping and the temperature increase, with the lowest values at 1000 K being just below 2 W m$^{-1}$ K$^{-1}$ for the nanowire $\kappa_{ph}$ in the $x$-direction and just above 1 W m$^{-1}$ K$^{-1}$ for the nanodot. For the nanowire, $\kappa_{ph}$ in the $x$-direction (across the barrier) is less than that in the $z$-direction (along the direction of the nanowire), which is expected since the presence of an interface in the $x$-direction should impede the flow of heat. At $T = 100$ K and large dopings, $\kappa_{ph}$ is noticeably larger for the nanodot than for the $\kappa_{xx}$ value of the nanowire. This is a result of the interface mass-mixing probability $\mathcal{P}$ value of 0.24 for the nanodot being smaller than 0.36 for the nanowire, since the effect disappears if interface scattering is neglected. Despite there being more interfaces in the nanodot system, the number of possible exchanges between sites in the nanodot and the bulk is smaller than it is in the case of the nanowire, as there are fewer atoms in the dot compared with the nanowire (that is, the volumetric fraction of Si, the constituent with higher $\kappa$, in the nanowire composite is larger than the volumetric fraction of nanodots in the nanodot composite). A similar effect has been observed in numerical comparisons of different volumetric fractions of Si nanowires[36,61] and also of Si nanodots in a Ge matrix.[35] However, even in the absence of interface mass-mixing scattering effects, nano-structuring effect will be observed due to the presence of the dual mass term in Eq. (11) and also due to its effects on the eigensolutions that represent the raw input to our calculation of $\kappa_{ph}$. Our prediction of the conductivity results of these ultrathin-period Si/Ge NW and ND superlattices is qualitatively consistent with previously reported results from other groups for thicker-period superlattices.[33,34] However, a direct numerical comparison of the results for different periodicity sizes, and obtained by employing different levels of theory, would be inappropriate.

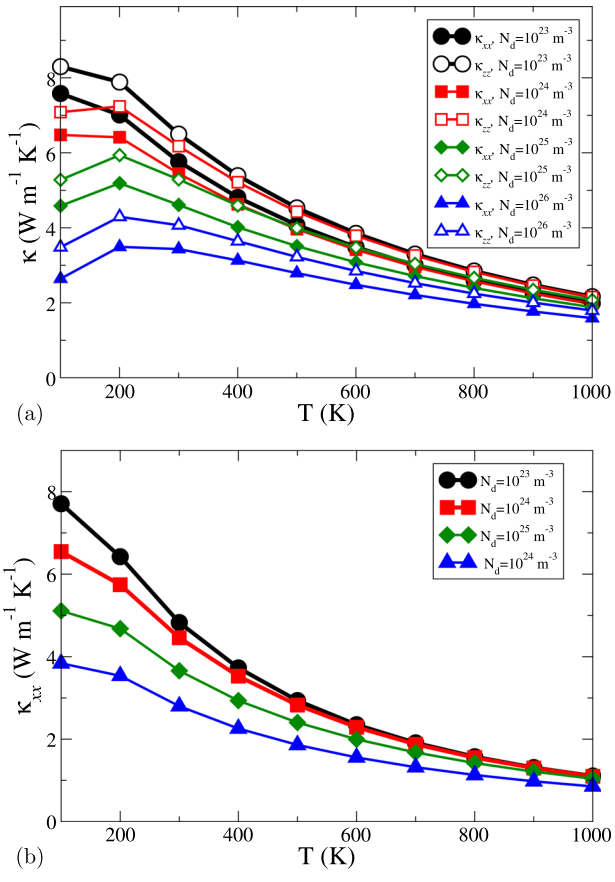


FIG. 4. Lattice contribution to the thermal conductivity for (a) nano-wires and (b) nanodots for a sample length of $3 \times 10^{-7}$ m.

It is also instructive to examine the effects of varying the sample size $L$ on the thermal conductivity. In Fig. 5 we display the effects of changing $L$ on the behavior of $\kappa_{ph}$ for the superlattice. At high-temperatures, the values of $\kappa_{ph}$ for $L = 3 \times 10^{-5}$ m and $L = 3 \times 10^{-6}$ m are also almost identical, indicating that at sufficiently large values of $L$ and $T$, $\kappa_{ph}$ becomes independent of sample size. However, this is not so at lower temperatures, where we find a much larger peak for the larger $L$ values, as we would expect since boundary scattering has strong effect in this region.[62] Results for the nanodot and nanowire are similar: Figure 6 shows that above 600 K, the $\kappa_{ph}$ values become insensitive to the nanowire sample sizes $L > 3 \times 10^{-7}$ m and nanodot sample sizes $L > 3 \times 10^{-6}$ m.

## IV. DISCUSSION

The presently reported reduction of $\kappa_{ph}$ due to increased interface scattering in ultrathin SLs receives favorable support from experimental measurements made on thin-period samples of $Bi_2Te_3/Sb_2Te_3$ (with $ZT = 2.5$)[10] and PbSnSe/PbSe.[18] In particular, the work by Jeffers *et al.*[18] echoes our prediction that the significant reduction in the cross-plane thermal conductivity of SLs of periods shorter than 5 nm is the result of stronger scattering of phonons by interfaces. To the best of our knowledge, there are no reports of the

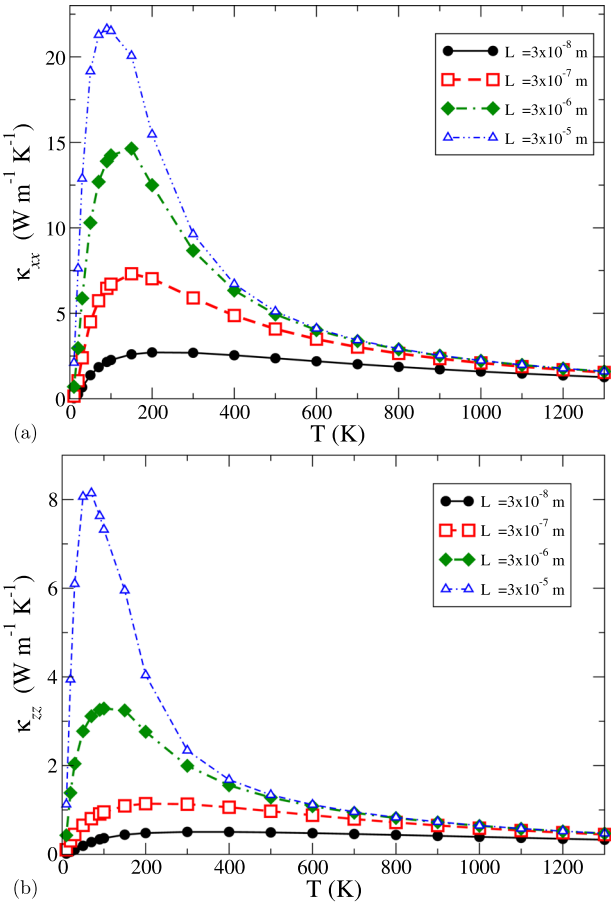


FIG. 5. Length dependence of phonon conductivity in the (a) $x$-direction and (b) $z$-direction for the (4,4) Si/Ge[001] superlattice with interface parameters $\alpha = 2.0$, $B = 1$, and $N_d = 10^{25}\,\mathrm{m}^{-3}$. (Results in the $y$-direction are similar to those in the $x$-direction.)

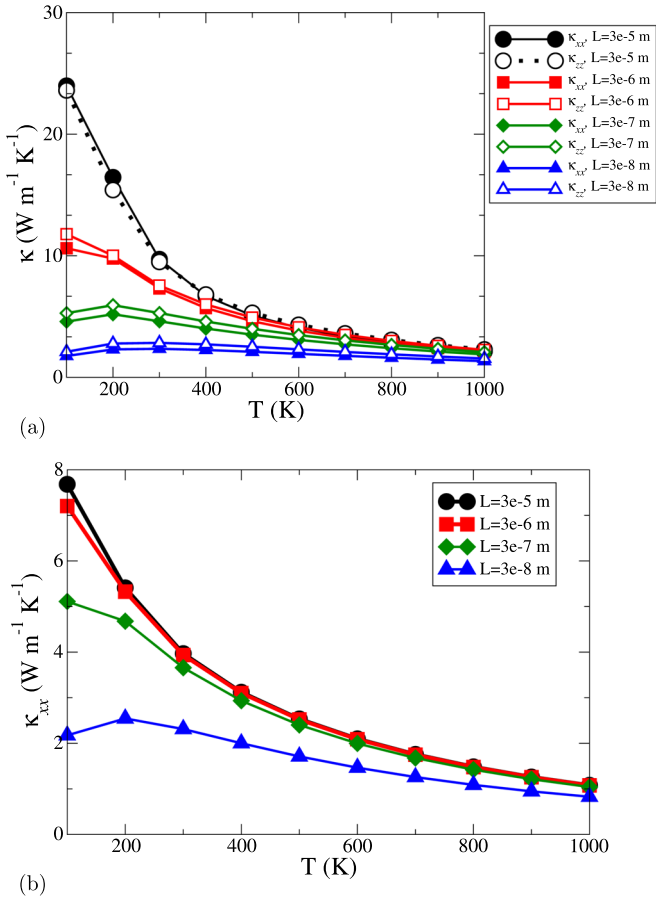


FIG. 6. Lattice thermal conductivity for different sample sizes of the (a) nanowire and (b) nanodot composite structures shown in Fig. 2, with $N_d = 10^{25}\,\mathrm{m}^{-3}$.

thermoelectric properties of Si/Ge ultrathin SL samples of the period sizes considered in this work. Therefore, at this stage it is difficult to quantify or gauge the effect of nanostructuring in enhancing $ZT$ via the reduction in $\kappa_{\mathrm{ph}}$. However, our results indicate that improving $ZT$ through nanostructure-induced reduction of $\kappa_{\mathrm{ph}}$ is a promising approach.

Accurate comparisons of the nanodot and nanowire results with the SL results are difficult as neither system is well converged. Moreover, the relative change in the cross-barrier results for different geometrical constructs for the nanocomposites (i.e., SL, NW, and ND) considered in this work depends strongly on two parameters:[29,35,37] volume fraction and the interface density of the insert (Si) within the matrix (Ge). Clearly, these parameters differ significantly for the SL, NW, and ND considered in our work. Nevertheless, we can confidently say that our predicted lattice thermal conductivities of the considered Si/Ge ultrathin nanocomposite structures are lower than that of structured or random $Si_xGe_{1-x}$ alloys[63] and amorphous-Si.[22] We expect similar comparative results between other nanocomposite structures and corresponding alloys or amorphous structures.

The lattice thermal conductivity of thicker-period nanocomposites is usually quantified by using two structural parameters: the insertion size and the insertion volume fraction $V_f$ (for Si embedded in the Ge host in the present case). These two parameters help define the interface density $\Phi$, with the conductivity varying as $\kappa_{\mathrm{ph}} \propto 1/\sqrt{\Phi}$.[37] Such a quantification of structural parameters is not very meaningful for ultrathin-period nanocomposites, e.g., those considered in this work. Instead, it is more meaningful to consider the ultrathin-period Si/Ge nanocomposites as new materials consisting of Si and Ge as two material mass (or density) patches within each unit cell, with the possibility of mixed atomic species at the internal interfaces, as has been done in this work. Using this picture one can describe the reduced thermal conductivity of the nanocomposites as a result mainly of a combination of the sample size dependence, the onset of *mini-Umklapp* three-phonon processes,[49] and from the interface mass-mixing. The phonon scattering rate from the interface mass-mixing is greater for thinner-period nanocomposites.[40] The combined effect of the *mini-Umklapp* and interface scatterings in a periodic nanocomposite structure is stronger than that achieved from the alloy formation. Consequently, the thermal conductivity of ultrathin-period nanocomposite structures is lower than the conductivity of an alloy formed by the same two material constituents (Si and Ge in the present case).

Notwithstanding these issues, the arrangement of the array of nanowires in the matrix is such that along the $x$-axis there exists a pathway through which heat can flow unimpeded by interfaces which is absent in the case of cross-

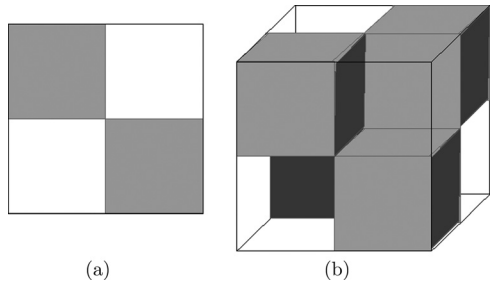


FIG. 7. Proposed array arrangements for (a) a checker-board array of nanowires (viewed from the top down) and (b) a staggered three-dimensional checker-board arrangement for nanodots as discussed in the text. Shaded squares (cubes) represent nanowires (nanodots); clear areas represent the matrix.

planar heat-flow in the superlattice, and so one might expect $\kappa_{ph}$ in the $x$-direction to be larger than that in the SL case. A similar argument applies in the case of the nanodot, where one might expect a decrease in a better converged result for $\kappa_{ph}$, but due to the existence of pathways in all three directions where heat can flow unimpeded by interfaces, this decrease might not reduce $\kappa_{ph}$ below the SL values. This would not be the case if the behavior of $\kappa_{ph}$ along the $xy$ face diagonal (nanowire) or the $xyz$ body diagonal (nanodot) were examined, where in an ideal case no pathway would be uninterrupted by an interface, but one might also consider other arrangements. Suitable examples would be a checker-board array of nanowires or a staggered 3D checker-board arrangement for nanodots (see Figure 7); these not only ensure that there is no cross-barrier direction where one can trace a path through the matrix that avoids the presence of an interface, but they also share the volumetric fraction of the equivalent superlattice, allowing a more simple comparison of the effects of interface scattering. This is still an idealization, since one might not be able to produce perfectly square nanowires or cubic quantum dots arranged in such a fashion, but it would provide some idea of how regularly spaced interfaces operating over the entirety of a nanostructure in more than one dimension might reduce $\kappa_{ph}$ and so improve $ZT$.

## V. CONCLUSION

In conclusion, the present investigation reveals that fabrication of a nanocomposite in the form of doped Si/Ge ultra-thin SLs produces results for the lattice thermal conductivity $\kappa_{ph}$ that are typically lower than the conductivities of SiGe alloys and of a-Si. This results from a combination of the sample length dependence, the onset of *mini-Umklapp* three-phonon processes, mass mixing at the interfaces between Si and Ge regions, and the sample doping level. The reduction of $\kappa_{ph}$ by dirty interfaces (modeled with the interface mass-mixing probability parameters $\alpha = 2.0$ and $\mathcal{B} = 1$) supports the phonon-glass electron-crystal concept[8,17] that has been advocated in the search for TE materials with enhanced $ZT$. It is possible that an improvement in the coefficient of performance for thermionic refrigerators[5,15] constructed from superlattices might also be observed due to the reduction of $\kappa_{ph}$ by both interface scattering and electron-phonon scattering.

Extending our theoretical approach for the superlattice structure, we have also examined the behavior of $\kappa_{ph}$ in ultra-thin nanodot and nanowire array structures. We have found that configurations of the kind discussed here do produce a reduction in $\kappa_{ph}$ relative to that found in bulk systems. However, our numerical results suggest that the reduction is not as pronounced as it is for the cross-planar SL conductivity. This may in part be due to a lack of convergence in our calculations (the improvement of which should be an aim of future investigations), but may also be due to the presence of pathways through the Ge matrix that are uninterrupted by interfaces. We have suggested some possible changes to the nanostructures that may address this problem.

## ACKNOWLEDGMENTS

We are grateful to the EPSRC (UK) for supporting this project via the Grant Award No.r EP/H046690/1. Quantum Espresso calculations were performed on the Intel Nehalem (i7) cluster (ceres) at the University of Exeter. I.O.T. also acknowledges support from the John Templeton Foundation as part of the Durham Emergence Project during the final stages of this work.

## APPENDIX: CALCULATING THE IMS PROBABILITY IN THREE DIMENSIONS

In the following, we provide a generalization of the procedure for calculating the mixing probability $\mathcal{P}$ in Ref. 43 to the three-dimensional unit cells used in this work to examine nanowire and nanodot systems.

Figure 8 gives a schematic illustration of the nanowire and nanodot cells under consideration. Each site in the system is labeled as follows: $l_\mu$ with $\mu = x, y, z$ labels the coordinates of a given atomic site within the cell, and $\tau_\mu$ labels the atomic sites that are part of the nanowire or of the nanodot (note that $\{\tau\} \subset \{\boldsymbol{l}\}$). A nanowire is equivalent to a nanodot with $\tau_z^{MAX} = l_z^{MAX}$, where $\tau_\mu^{MAX}$ and $l_\mu^{MAX}$ are the largest values of $\tau_\mu$ or $l_\mu$ in the direction $\mu$. A "site" is taken to be the location or potential location of a pair of atoms similar to the bilayers of the superlattice case; we take interface mixing to involve the exchange of a pair of basis atoms in

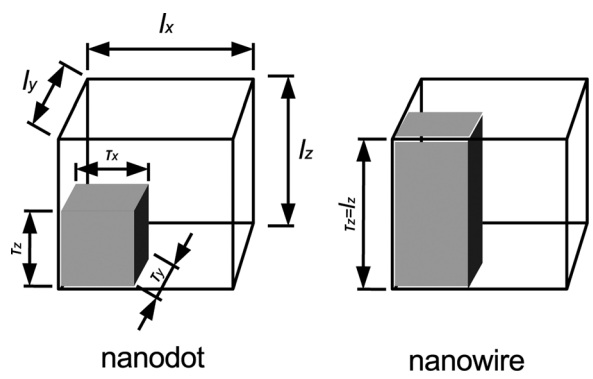


FIG. 8. Schematic of a nanowire and nanodot cell. The filled region represents the wire or dot and the unfilled region is the matrix.

the bulk diamond structure for Si and Ge within the nanostructure with a pair external to it. The cells under consideration consist of a three dimensional cubic lattice with pairs occupying every other site.

We begin with a generalization of equation (A3) in Ref. 43 to three dimensions:

$$\mathbb{P}^{\tau\boldsymbol{l}}_{\mathrm{OCC}} = \frac{1}{8N_{\mathrm{SWAP}}} \sum_{i}^{8} \frac{1}{(S-3+\mathcal{B})^{\alpha}}, \tag{A1}$$

where $N_{\mathrm{SWAP}} = \frac{1}{2} l_X l_y l_z$ is the number of occupied sites, $\mathcal{B}^{\alpha}$ is a parameter determining the deviation of the probability of swapping at the interface from what one would expect given the principle of indifference, and where $S = \sqrt{\sum_{j=x,y,z} (||\tau_j - l_j| - d_{i,j}| - X_j)^2}$. The $\boldsymbol{d}_i$ are vectors included to account for the periodicity of the system:

$$\begin{aligned}
&\boldsymbol{d}_1 = (0,0,0); \quad \boldsymbol{d}_2 = (l_x^{\mathrm{MAX}},0,0), \quad \boldsymbol{d}_3 = (0,l_y^{\mathrm{MAX}},0),\\
&\boldsymbol{d}_4 = (0,0,l_z^{\mathrm{MAX}}); \quad \boldsymbol{d}_5 = (l_x^{\mathrm{MAX}},l_y^{\mathrm{MAX}},0),\\
&\boldsymbol{d}_6 = (l_x^{\mathrm{MAX}},0,l_z^{\mathrm{MAX}}), \quad \boldsymbol{d}_7 = (0,l_y^{\mathrm{MAX}},l_z^{\mathrm{MAX}});\\
&\boldsymbol{d}_8 = (l_x^{\mathrm{MAX}},l_y^{\mathrm{MAX}},l_z^{\mathrm{MAX}}).
\end{aligned} \tag{A2}$$

The value of $\mathbf{X}$ depends on the presence or absence of an interface between the two points in a given direction. For nanowires, $\boldsymbol{X} = \mathbf{0}$ unless:

- If $\tau_i < l_i$ and $l_i > l_j$ where $i, j = x, y$ and $i \neq j$, then $X_i = 1$ and all other components of $\boldsymbol{X}$ are zero.
- If $\tau_x = \tau_y$ and $l_x = l_y$ then $X_x = X_y = 1$ and $X_z = 0$.

For nanodots, $\boldsymbol{X} = \mathbf{0}$ unless:

- If $\tau_i < l_i$, $l_i > l_j$ and $l_x > l_z$ where $i, j = x, y$ and $i \neq j$, then $X_i = 1$ and all other components of $\boldsymbol{X}$ are zero.
- If $\tau_z < l_z$, $l_z > l_x$ and $l_z > l_y$ then $X_z = 1$ and all other components of $\boldsymbol{X}$ are zero.
- If $\tau_x = \tau_y$, $l_x = l_y$ and $l_x > \tau_x^{\mathrm{MAX}}$ then $X_x = X_y = 1$ and $X_z = 0$.
- If $\tau_z = \tau_i$, $l_z = l_i$ and $l_z > \tau_z^{\mathrm{MAX}}$ where $i = x, y$ then $X_z = X_i = 1$ and the remaining component of $\boldsymbol{X}$ is zero.
- If $\tau_z = \tau_x = \tau_y$, $l_z = l_x = l_y$, and $l_z > \tau_z^{\mathrm{MAX}}$ then $\mathbf{X} = \mathbf{1}$.

We now define the probability of exchange between site $\boldsymbol{\tau}$ and site $\boldsymbol{l}$ as:

$$\mathbb{P}^{\tau\boldsymbol{l}}_{\mathrm{SWAP}} = \begin{cases} \mathbb{P}^{\tau\boldsymbol{l}}_{\mathrm{OCC}} & \text{if } \boldsymbol{\tau} \text{ and } \mathbf{l} \text{ are occupied} \\ 0 & \text{otherwise.} \end{cases} \tag{A3}$$

Following Ref. 43, we now calculate the probability that site $\boldsymbol{\tau}$ within the nanoparticle (*viz.* the insert) exchanges with site $\boldsymbol{l}$ within the matrix:

$$\mathbb{P}^{\tau}_{\mathrm{SWAP}} = \sum_{\boldsymbol{l} \notin \{\tau\}} \mathbb{P}^{\tau\boldsymbol{l}}_{\mathrm{SWAP}}, \tag{A4}$$

the probability that it does not exchange

$$\mathbb{P}^{\tau}_{\mathrm{NOSWAP}} = 1 - \mathbb{P}^{\tau}_{\mathrm{SWAP}}, \tag{A5}$$

the probability that no sites at all are exchanged

$$\mathbb{P}_{\mathrm{NOSWAP}} = \prod_{\text{occupied } \tau \text{ sites}} \mathbb{P}^{\tau}_{\mathrm{NOSWAP}}, \tag{A6}$$

and hence the overall value of $\mathcal{P}$

$$\mathcal{P} = 1 - \mathbb{P}_{\mathrm{NOSWAP}}. \tag{A7}$$

Note that our use of $\mathcal{P}$ in Eq. (15) is a simplification; in general one would have a more complicated expression for the overall IMS probability, which we have replaced with an overall approximation. However, given that there is no known *a priori* model for interface "dirtiness" with to begin with, we feel that making this replacement is justified, will be simpler to implement for more complex systems, and will capture much of the relevant qualitative behavior. We should add that with respect to the $\boldsymbol{d}$ vectors, which account for the periodicity of the system, more could be included in order to account for swaps from cells that are further afield, but unless $\alpha$ is chosen so that the decay of $\mathbb{P}^{\tau\boldsymbol{l}}_{\mathrm{OCC}}$ with distance is very gradual, this should not have much effect.


[1] S. Berber, Y.-K. Kwon, and D. Tomànek, Phys. Rev. Lett. **84**, 4613 (2000).
[2] D. L. Nika, E. P. Pokatilov, A. S. Askerov, and A. A. Balandin, Phys. Rev. B **79**, 155413 (2009).
[3] W. Kim, R. Wang, and A. Majumdar, Nano Today **2**, 40 (2007).
[4] C. Wood, Energy Convers. Manage. **24**, 317 (1984).
[5] G. D. Mahan, J. D. Sofo, and M. Bartkowiak, J. Appl. Phys. **83**, 4683 (1998).
[6] F. J. DiSalvo, Science **285**, 703 (1999).
[7] G. Chen, M. S. Dresselhaus, G. Dresselhaus, J.-P. Fleurial, and T. Caillat, Int. Mater. Rev. **48**, 45 (2003).
[8] H. J. Goldsmidt, *Introduction to Thermoelectricity* (Springer-Verlag, Berlin, 2010).
[9] L. D. Hicks and M. S. Dresselhaus, Phys. Rev. B **47**, 16631 (1993).
[10] R. Venkatasubramanian, E. Siivola, T. Colpitts, and B. O'Quinn, Nature **413**, 597 (2001).
[11] A. I. Hochbaum, R. Chen, R. D. Delgado, W. Liang, E. C. Garnett, M. Najarian, A. Majumdar, and P. Yang, Nature **451**, 163 (2008).
[12] A. I. Boukai, Y. Bunimovich, J. Tahir-Keli, J.-K. Yu, W. A. Goddard III, and J. R. Heath, Nature **451**, 168 (2008).
[13] A. J. Minnich, M. S. Dresselhaus, Z. F. Ren, and G. Chen, Energy Environ. Sci. **2**, 466 (2009).
[14] V. Goyal, D. Teweldebrhan, and A. A. Balandin, Appl. Phys. Lett. **97**, 133117 (2010).
[15] P. Pichanusakorn and P. Banadau, Mater. Sci. Eng. **R67**, 19 (2010).
[16] W. Liu, X. Yan, and Z. Ren, Nano Energy **1**, 42 (2012).
[17] G. Slack, in *CRC Handbook of Thermoelectrics*, edited by D. M. Rowe (CRC Press, Boca Raton, 1994), p. 407.
[18] J. D. Jeffers, K. Namjou, Z. Cai, P. J. McCann, and L. Olona, Appl. Phys. Lett. **99**, 041903 (2011).
[19] C. Glassbrenner and G. Slack, Phys. Rev. **134**, A1058 (1964).
[20] D. A. Broido and T. L. Reinecke, Phys Rev B **64**, 045324 (2001).
[21] J. P. Heremans, B. Wiendlocha, and A. M. Chamoire, Energy Environ. Sci. **5**, 5510 (2012).
[22] S.-M. Lee, D. G. Cahill, and R. Venkatasubramanian, Appl. Phys. Lett. **70**, 2957 (1997).
[23] T. Borca-Tascuic, W. Liu, T. Zeng, D. W. Song, C. D. Moore, G. Chen, K. L. Wang, M. S. Goorsky, T. Radetic, R. Gronsky, T. Koga, and M. S. Dresselhaus, Superlattices Microstruct. **28**, 199 (2000).
[24] S. T. Huxtable, A. R. Abramson, A. Majumdar, A. Shakouri, and E. T. Croke, in *Proceedings of 2002 ASME International Mechanical Engineering Congress and Exposition* (2002), Paper No. IMECE2002-34239, p. 1.
[25] D. Li, Y. Wu, R. Fan, P. Yang, and A. Majumdar, Appl. Phys. Lett. **83**, 3186 (2003).
[26] J. R. Sootsman, R. J. Pcionek, H. Kong, C. Uher, and M. G. Kanatzidis, Chem. Mater. **18**, 4993 (2006).
[27] J. Androulakis, C.-H. Lin, H.-J. Kong, C. Uher, C.-I. Wu, T. Hogan, B. A. Cook, T. Caillat, K. M. Paraskevopoulos, and M. G. Kanatzidis, J. Am. Chem. Soc. **129**, 9780 (2007).

[28]C. Dames and G. Chen, J. Appl. Phys. **95**, 682 (2004).
[29]A. Minnich and G. Chen, Appl. Phys. Lett. **91**, 073105 (2007).
[30]X. Lu and J. Chu, J. Appl. Phys. **101**, 114323 (2007).
[31]J. Garg and G. Chen, Phys. Rev. B **87**, 140302(R) (2013).
[32]G. Pernot, M. Stoffel, I. Savic, F. Pezzoli, P. Chen, G. Savelli, A. Jacquot, J. Schumann, U. Denker, I. Mönch, Ch. Deneke, O. G. Schmidt, J. M. Rampnoux, S. Wang, M. Plissonnier, A. Rastelli, S. Dilhaire, and N. Mingo, Nat. Mater. **9**, 491 (2010).
[33]D. L. Nika, E. P. Pokatilov, A. A. Balandin, V. M. Fomin, A. Rastelli, and O. G. Schmidt, Phys. Rev. B **84**, 165415 (2011).
[34]D. L. Nika, A. I. Cocemasov, D. V. Crismari, and A. A. Balandin, Appl. Phys. Lett. **102**, 213109 (2013).
[35]A. Behrang, M. Grmela, C. Dubois, S. Turenne, and P. G. Lafleur, J. Appl. Phys. **114**, 014305 (2013).
[36]A. Behrang, M. Grmela, C. Dubois, S. Turenne, P. G. Lafleur, and G. Lebon, Appl. Phys. Lett **104**, 063106 (2014).
[37]J. Al-Otaibi and G. P. Srivastava, J. Phys.: Condens. Matter **28**, 145304 (2016).
[38]W. S. Capinski, H. J. Maris, T. Ruf, M. Cardona, K. Ploog, and D. S. Katzer, Phys. Rev. B **59**, 8105 (1999).
[39]M. V. Simkin and G. D. Mahan, Phys. Rev. Lett. **84**, 927 (2000).
[40]S. P. Hepplestone and G. P. Srivastava, Phys. Rev. B **82**, 144303 (2010).
[41]S. P. Hepplestone and G. P. Srivastava, Phys. Rev. B **84**, 115326 (2011).
[42]I. O. Thomas and G. P. Srivastava, Phys. Rev. B **86**, 045205 (2012).
[43]I. O. Thomas and G. P. Srivastava, Phys. Rev. B **88**, 115207 (2013).
[44]I. O. Thomas and G. P. Srivastava, Phys. Rev. B **87**, 085410 (2013).
[45]G. P. Srivastava, J. Phys. Chem. Solids **41**, 357 (1980).
[46]J. Garg, N. Bonini, and N. Marzari, in *Length-Scale Dependent Phonon Interactions*, edited by S. L. Shindé and G. P. Srivastava (Springer, New York, 2014), Chap. 4.
[47]N. Mingo, D. A. Stewart, D. A. Broido, L. Lindsay, and W. Li, in *Length-Scale Dependent phonon Interactions*, edited by S. L. Shindé and G. P. Srivastava (Springer, New York, 2014), Chap. 5.
[48]G. P. Srivastava, *The Physics of Phonons* (Taylor and Francis, New York, 1990).
[49]S. Y. Ren and J. D. Dow, Phys. Rev. B **25**, 3750 (1982).
[50]I. O. Thomas and G. P. Srivastava, IOP Conf. Ser.: Mater. Sci. Eng. **68**, 012007 (2014).
[51]C. Kittel, *Introduction to Solid State Physics*, 7th ed. (Wiley, New York, 1996).
[52]P. Gianozzi, S. Baroni, N. Bonini, M. Calandra, R. Car, C. Cavazzoni, D. Ceresoli, G. L. Chiarotti, M. Cococcioni, I. Dabo, and A. Dal Corso, J. Phys.: Condens. Matter **21**, 395502 (2009); See http://www.quantum-espresso.org for code and further details.
[53]See http://www.quantum-espresso.org for the pseudopotentials Si.pz-vbc.UPF and Ge.pz-bhs.UPF.
[54]H. J. Monkhorst and J. D. Pack, Phys. Rev. B **13**, 5188 (1976).
[55]M. T. Yin and M. L. Cohen, Phys. Rev. B **26**, 3259 (1982).
[56]W. B. Gauster, J. Appl. Phys. **44**, 1089 (1973).
[57]See http://www.jmol.org/ for Jmol: An open-source Java viewer for chemical structures in 3D.
[58]www.quantum-espresso.org/wp_content/uploads/Doc/ph_usr_guide/node10.html (last accessed December 16, 2014).
[59]Y.-W. Mo, D. E. Savage, B. S. Swartzentruber, and M. G. Lagally, Phys. Rev. Lett. **65**, 1020 (1990).
[60]T. Ma, H. Tu, B. Shao, A. Liu, and G. Hu, Mater. Sci. Semicond. Process. **9**, 49 (2006).
[61]R. Yang, G. Chen, and M. Dresselhaus, Phys. Rev. B **72**, 125418 (2005).
[62]M. N. Luckyanova, Science **338**, 936 (2012).
[63]J. Garg, N. Bonini, B. Kozinsky, and N. Marzari, Phys. Rev. Lett. **106**, 045901 (2011).